Infrared and Microwave Spectra of the N2–propyne dimer

ARTICLE *in* JOURNAL OF MOLECULAR SPECTROSCOPY · JANUARY 1997

Impact Factor: 1.48

7 AUTHORS, INCLUDING:

Shao-Hsuan Tseng

University of Stirling

5 PUBLICATIONS **22** CITATIONS

SEE PROFILE

Francis J. Lovas

National Institute of Standards and T…

287 PUBLICATIONS **9,073** CITATIONS

SEE PROFILE

JOURNAL OF MOLECULAR SPECTROSCOPY **182,** 132–147 (1997)
ARTICLE NO. MS967193

Infrared and Microwave Spectra of the N_2–Propyne van der Waals Cluster

Shao-Hui Tseng,*[,1] David F. Eggers,*[,2] Thomas A. Blake,*[,3] Rainer Beck,*[,4] R. O. Watts,*[,5] F. J. Lovas,† and N. Zobov†[,6]

*Department of Chemistry, University of Washington, Mail Stop BG-10, Seattle, Washington 98195-2145; and †National Institute of Standards and Technology, Optical Technology Division, Building 221, Room B208, Gaithersburg, Maryland 20899

Received August 5, 1996; in revised form September 24, 1996

The infrared spectrum of $^{14}N_2$–CH_3CCH in the 3.0-μm region has been observed and the rovibrational transitions have been assigned for the A ($m = 0$) and E ($m = \pm 1$) methyl top internal rotor states of this near slipped parallel van der Waals molecule. The E-state transitions were used to estimate the barrier to internal rotation as 10 cm^{-1}. The observed A-state microwave transitions of $^{14}N_2$–CH_3CCH, $^{15}N_2$–CH_3CCH, and $^{15}N_2$–CH_3CCD are split into doublets. This doublet splitting, which is too small to be observed in the infrared spectrum, is attributed to the internal motion of the N_2 moiety about an axis connecting the centers-of-mass of the molecules in the cluster; i.e., the N_2 molecule rotates out of the heavy atom plane of the cluster. The splittings in the microwave spectra were fit to a barrier height of 71 cm^{-1} for the hindered N_2 motion.

INTRODUCTION

In a recent paper we reported the structures of the N_2–CH_3CCH and CO–CH_3CCH van der Waals clusters based on a preliminary analysis of the infrared and microwave spectra (*1*). Sufficient microwave data for isotopic variants of the clusters allowed for the fitting of the parameters required to uniquely determine their structures. The experimental geometries of the complexes have the heavy atoms of the clusters lying in a plane and the N_2 and CO center-of-mass vectors approximately perpendicular to the symmetry axis of the propyne unit with center-of-mass separations of 3.708(2) and 3.756(1) Å, respectively. These structures are analogous to the T-shaped structures of the rare gas complexes Ar–CH_3CCH (*2*), Ar–CH_3Cl (*3*), and Ar–CH_3CN (*4*). Each of these rare gas complexes exhibit A and E symmetry states, which arise from nearly free internal rotation of the methyl symmetric top unit with barriers on the order of 20 cm^{-1} or less. The infrared spectrum of N_2–CH_3CCH also exhibits internal rotation splitting from the nearly free internal rotation of the methyl top, and the microwave spectra of the A-state for the $^{14}N_2$–propyne and $^{15}N_2$–propyne complexes also show splittings which we interpret as arising from the internal rotation of the nitrogen molecule in the complex.

In the present paper we provide a detailed analysis of the infrared and microwave spectra of N_2–propyne with a treatment of the barriers to internal rotation of each subunit in the complex. Values of barriers to methyl and N_2 internal rotation are also determined.

EXPERIMENT

Infrared spectra of N_2–CH_3CCH were measured using a computer-controlled F-center laser and a differentially pumped molecular beam apparatus with optothermal detection. Specific details of this apparatus are given elsewhere (*2, 5*). A brief description of the current study is given here. A mixture consisting of about 1% by volume CH_3CCH and 5% by volume N_2 in helium was expanded through a 50-μm, room-temperature nozzle at a backing pressure of 1000 kPa. The molecular beam was collimated using a 190-μm skimmer. The molecular beam then passed between two parallel, gold-coated mirrors, placed about 25 cm in front of the bolometer detector. The mirrors allow the molecular beam to be multiply crossed with the infrared radiation from the F-center laser. A silicon-on-sapphire bolometer cooled to 1.8 K was used to monitor the energy flux of the molecular beam. The bolometer has an NEP of $\sim 2 \times 10^{-14}$ $W/\sqrt{Hz}$ and a time constant of 3 ms. The laser radiation was chopped

[1] Present address: Department of Molecular Biotechnology, Fluke Hall, University of Washington, Box 357730, Seattle, WA 98195-2145.
[2] Deceased.
[3] Permanent address: Battelle/Pacific Northwest National Laboratory, P.O. Box 999, Mail Stop K3-58, Richland, WA 99352.
[4] Permanent address: Institute de Chimie Physique Moleculaire, Ecole Polytechnique Federal de Lausanne, CH-1015 Lausanne, Switzerland.
[5] Permanent address: School of Chemistry, The University of Melbourne, Parkville, Victoria 3052, Australia.
[6] Permanent address: Institute of Applied Physics, Nizhny, Novgorod, Russia.

0022-2852/97 $25.00

at ~100 Hz and the amplified bolometer signal was monitored with a lock-in amplifier for phase-sensitive detection. With optimal alignment through the multipass cell, an instrumental resolution of 10 MHz was obtained. Frequency calibration of the cluster spectra was accomplished by using the CH_3CCH monomer spectrum (*2, 6, 7*).

The microwave apparatus and methods followed closely those described in our earlier work on Ar–CH_3CCH (*2*). Spectra were recorded using a Balle–Flygare-type (*8, 9*) Fourier transform microwave spectrometer at the National Institute of Standards and Technology. A dual-inlet pulsed solenoid valve delivered a supersonic molecular beam from a mixture of about 1% by volume N_2 and about 1% by volume CH_3CCH entrained in separate samples with Ar carrier gas, at a total pressure of 100 kPa (1 atm) to the center of the Fabry–Perot cavity. The dual inlet flow nozzle allowed each component to be shut off independently in order to determine if the observed spectral lines required both chemical species, i.e., N_2 and CH_3CCH. Thus, spectra from other dimers, e.g., Ar–CH_3CCH, could be readily eliminated. Typically, the microwave spectrum was recorded at a resolution of 4 kHz. The *d1*-propyne sample was prepared at the University of Washington and sent to the NIST laboratories. The isotopic species $^{15}N_2$ was from a commercial source.

RESULTS AND DISCUSSION

As in the case of Ar–CH_3CCH, the infrared spectrum of N_2–CH_3CCH in the region of the ν_1 band of the monomer at 3.0 μm exhibits transitions in both the $m = 0$ (A) and the $|m| = 1$ (E) states, where m is the angular momentum quantum number for the internal rotation of the methyl top about propyne's symmetry axis. The very small cross section for nuclear spin conversion of the methyl group protons maintains population in the $|m| = 1$ state even at a jet rotational temperature of ~1 K. Figures 1 and 2 show portions of the observed high-resolution infrared spectrum of the N_2–CH_3CCH complex. The frequencies, assignments, and observed-minus-calculated frequencies for the 64 A-state transitions are listed in Table 1. All of the assigned A-state transitions are b types which is consistent with a cluster structure that has the acetylenic C–H stretch vibrational dipole moment pointing predominantly along the b axis of the cluster. Initially, four $^RQ_0$ and six $^PQ_1$ transitions were assigned based on a simulation of the spectra from a ''guess'' of the structure: their strong intensity and regular spacing about the band origin of the cluster made their assignment straightforward. Subsequently, transitions from $^PP_1$, $^RP_0$, $^RR_0$, $^PR_1$, $^RR_1$, $^RR_2$, $^RQ_1$, and $^PQ_2$ subbands were assigned. To check the assignment, 25 ground state combination differences (GSCDs) were calculated from the assigned infrared transitions and fit to the constants of a Watson A-reduction Hamiltonian (*10*). The fit RMS deviation is 0.00047 cm^{-1} with three GSCDs slightly larger than this. The GSCDs are listed in Table 2. These data were subsequently used to aid in the searches for the corresponding microwave transitions.

Forty-two E-state transitions were assigned in the infrared spectra and are listed in Table 3. Among these are 27 b-type transitions, 8 c-type transitions, and 7 transitions that do not appear to obey standard asymmetric rotor a-, b-, or c-type selection rules. A similar situation was observed in the spectrum of Ar–CH_3CCH and is due to the strong mixing of rotational energy levels via the Coriolis interaction between the total angular momentum, **J**, excluding nuclear spins, and that of the internal rotor (*3*). As in the case of Ar–CH_3CCH, there is a pileup of E-state transitions near the band origin that obey the selection rule $|J, K_a, K_c\rangle \leftarrow |J, K_a, K_c\rangle$. This pileup is the most intense feature of the spectrum. From the E-state data set, 33 GSCDs can be found from which seven identical pairs of GSCDs were formed from different infrared transitions (see Table 4). Four of these pairs agree within experimental uncertainty while the other three have slightly larger differences of about 0.0007 cm^{-1}.

While the infrared spectrum clearly shows evidence for the presence of A- and E-states from the internal rotation of the methyl group, only the A-state of the complex was sought in the microwave range. (From our experience with the microwave spectrum of Ar–CH_3CCH and the anticipated quadrupole hyperfine splitting in $^{14}N_2$–CH_3CCH, it was assumed that the E-state transitions of this complex would present difficulties in the analysis due to the complex hyperfine structure and the weakness of the spectrum.) Initial searches of the microwave transitions were based on predictions from a preliminary analysis of the infrared spectrum of $^{14}N_2$–CH_3CCH. When these line centers were scanned, two clusters of hyperfine components separated by several megahertz were found. The higher frequency group was about twice as intense as the lower frequency group. Since the separation of the two groups is too small to be explained by the internal rotation of the methyl group, we conclude that this small splitting arises from the internal rotation of the N_2 molecule in the complex, much like the N_2–HOH complex exhibits (*11*). We could not find evidence of the N_2 tunneling splitting in the infrared spectrum.

The permutation-inversion group for N_2–propyne is G_{12} and we will use the irreducible representations for the isomorphic D_6 group to label the internal rotor states of the cluster. Since no splitting due to the N_2 internal rotor is observed in the infrared spectrum, we label transitions in that spectrum as belonging to either A or E methyl internal rotor states. In the microwave spectrum we label states as being either A or B N_2 internal rotor states, where the A-state possesses a symmetric N_2 nuclear spin wavefunction and the B-state possesses an antisymmetric N_2 nuclear spin state. Keep in mind that both of these states correlate to the A ($m = 0$) methyl internal rotor state. In order to verify this

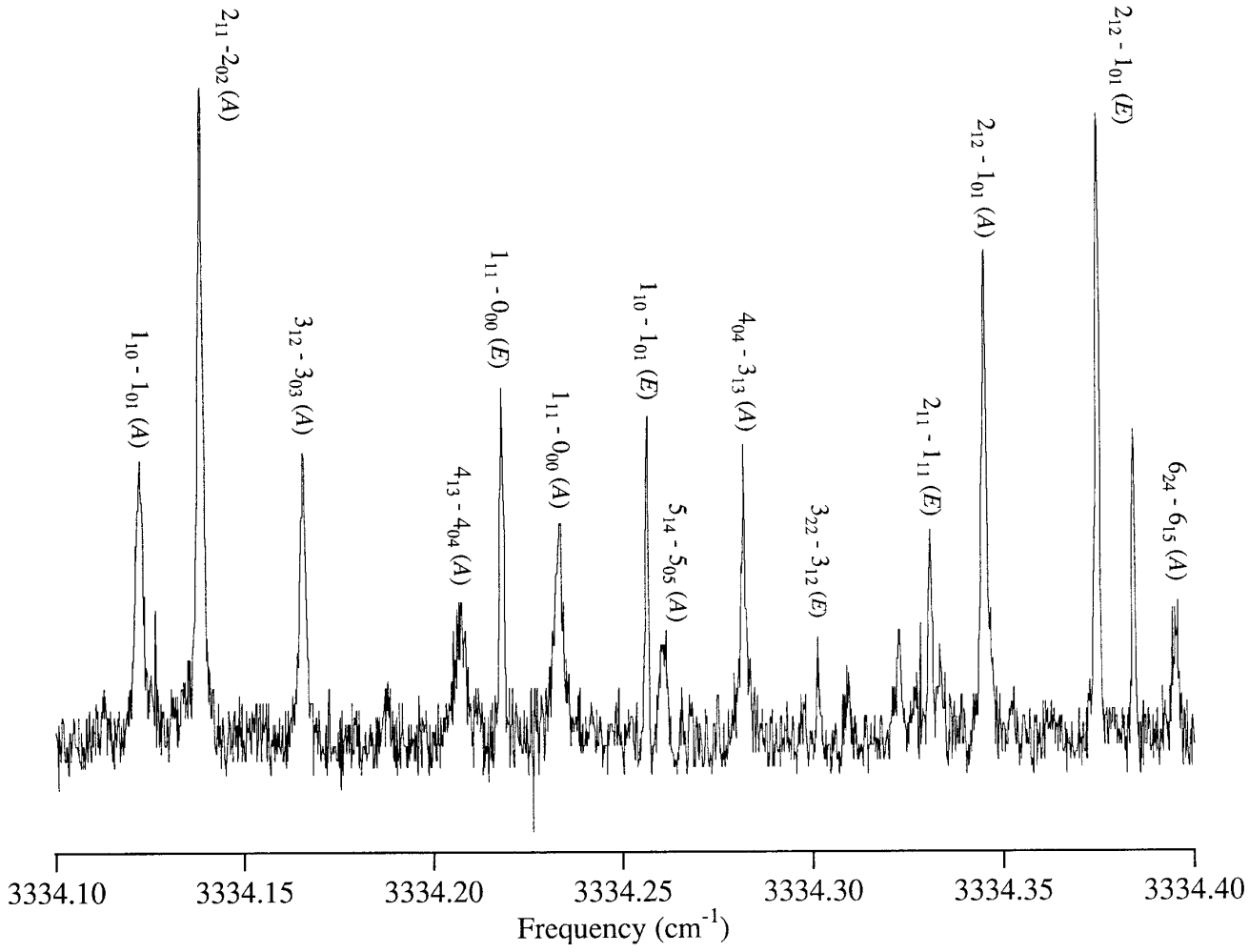

FIG. 1. A portion of the *A*-state *Q*-branch region of the infrared spectrum of $^{14}N_2$–CH_3CCH.

interpretation, the microwave spectrum of the $^{15}N_2$–CH_3CCH complex was taken and assigned. (In this work we have used only the homonuclear species $^{15}N^{15}N$ and $^{14}N^{14}N$.) The $^{15}N_2$ complex also exhibited two transitions, but with a 3/1 intensity ratio. The intensity ratios were consistent with a model that interchanges the nitrogen atoms, ^{14}N with nuclear spin 1 and ^{15}N with spin $\frac{1}{2}$. For $^{14}N_2$ the nuclear spin statistical weight is $g = 6$ for the *A*-state ($I = 0, 2$) and $g = 3$ for the *B*-state ($I = 1$), and for the $^{15}N_2$ species the spin weight is $g = 1$ for the *A* state ($I = 0$) and $g = 3$ for the *B*-state ($I = 1$). The observed transition frequencies of the *A*- and *B*-states of $^{14}N_2$–CH_3CCH are listed in Tables 5 and 6, respectively, with the centers-of-gravity for the hyperfine transitions of both states listed in Table 7. The observed transition frequencies of the *A*- and *B*-states of $^{15}N_2$–CH_3CCH are listed in Table 8. The microwave spectrum of the $^{15}N_2$–CH_3CCD species was also measured and provided resolved hyperfine structure for the D nucleus which is shown in Tables 9 and 10. Our limited $^{15}N_2$ sample was depleted before accurate predictions of *E*-state transitions were obtained.

To fit the $^{14}N_2$–CH_3CCH infrared data we use a refined set of ground state spectroscopic constants determined from the microwave spectrum, so we will begin with an analysis of those data. The Hamiltonian used to fit these data is shown in the following equation and the matrix elements are set up with a Watson *A*-reduction in an I^r representation (*10*):

$$\begin{aligned} H = H_{\text{rot}} + H_Q = {} & [A - \tfrac{1}{2}(B + C)]\mathbf{J}_a^2 + \tfrac{1}{2}(B + C)\mathbf{J}^2 \\ & + \tfrac{1}{2}(B - C)(\mathbf{J}_b^2 - \mathbf{J}_c^2) - \Delta_J\mathbf{J}^4 - \Delta_{JK}\mathbf{J}^2\mathbf{J}_a^2 \\ & - \Delta_K\mathbf{J}_a^4 - 2\delta_J\mathbf{J}^2(\mathbf{J}_b^2 - \mathbf{J}_c^2) - \delta_K[\mathbf{J}_a^2(\mathbf{J}_b^2 - \mathbf{J}_c^2) \\ & + (\mathbf{J}_b^2 - \mathbf{J}_c^2)\mathbf{J}_a^2] + 2f(I, J, F)[eQq_{aa}\langle\mathbf{J}_a^2\rangle \\ & + eQq_{bb}\langle\mathbf{J}_b^2\rangle + eQq_{cc}\langle\mathbf{J}_c^2\rangle]/[J(J + 1)]. \end{aligned} \quad [1]$$

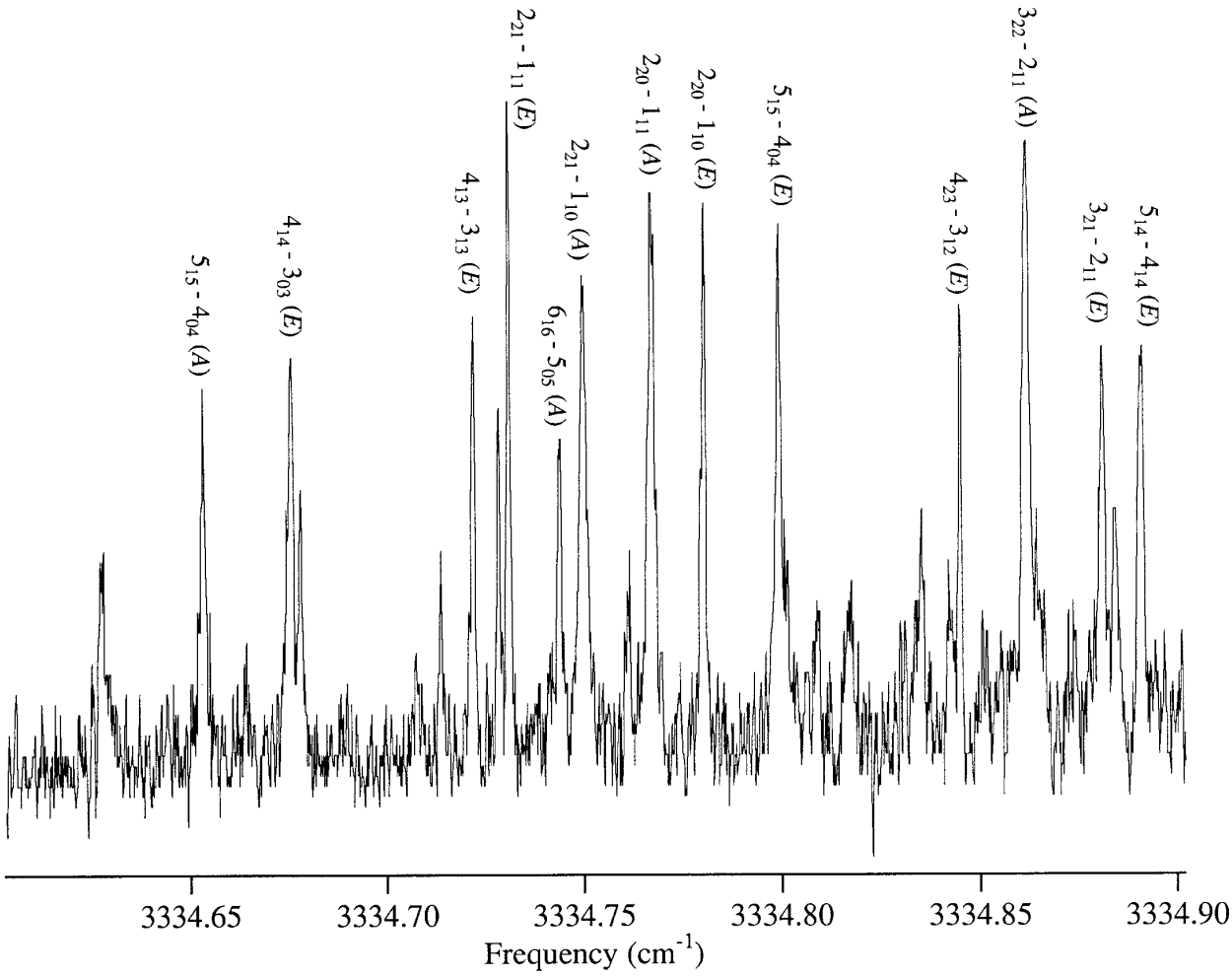

FIG. 2. A portion of the *E*-state *R*-branch region of the infrared spectrum of $^{14}N_2$–CH_3CCH.

The hyperfine analysis follows the method described by Kirchhoff and Johnson (*12*). A variational calculation is used to compute the eigenvectors and energies of the Hamiltonian using a direct product of the rigid rotor eigenvectors and the quadrupole eigenvectors $|F\rangle$ to form the basis set, where $\mathbf{F} = \mathbf{I} + \mathbf{J}$ and $f(I, J, F)$ is Casimir's function. The rotational constants A, $(B + C)/2$, and $(B - C)/2$, the five quartic distortion constants, and the three quadrupole coupling constants eQq_{aa}, eQq_{bb}, and eQq_{cc} for the A and B-states of $^{14}N_2$–CH_3CCH are given in Table 11. The fit values for $^{15}N_2$–CH_3CCH are given in Table 12 and those of $^{15}N_2$–CH_3CCH are given in Table 13. Since only three rotational transitions were observed for $^{15}N_2$–CH_3CCD it is not possible to determine the uncertainty of the constants reported; a conservative estimate of this uncertainty would be 5 kHz. The fit A-state rotational and quadrupole constants of these isotopic species were used to calculate the structure of the cluster. Details of the structure calculation are given in Ref. (*1*).

In our fitting processes we fit to the sum and difference combinations of B and C, that is, $(B + C)/2$ and $(B - C)/2$, rather than B and C separately. All other molecular constants are fit separately. There are several reasons for this choice: first, the uncertainty in $(B + C)/2$ is usually significantly less than the uncertainty in $(B - C)/2$. For instance, in the B-state microwave transitions of $^{15}N_2$–CH_3CCH the $(B + C)/2$ uncertainty is almost an order of magnitude less than that for $(B - C)/2$. Also, the $(B + C)/2$ uncertainty is substantially smaller than that of either B or C when they are fit separately. Second, the correlation matrix has smaller off-diagonal entries when fitting $(B + C)/2$ and $(B - C)/2$. From this same data set we find that fitting B and C separately gives a correlation between them of 0.989, while fitting $(B + C)/2$ and $(B - C)/2$ gives the $(B + C)/2 - (B - C)/2$ correlation as only 0.588. Similarly, the correlations of B and C with the other constants are generally larger than those for $(B + C)/2$ and $(B - C)/2$ with the corresponding constants.

TABLE 1
Observed *A*-State Infrared Transitions of $^{14}N_2$–CH_3CCH (cm^{-1})

Upper			Lower			Observed		Upper			Lower			Observed	
J	*Ka*	*Kc*	*J*	*Ka*	*Kc*	Frequency	o - c	*J*	*Ka*	*Kc*	*J*	*Ka*	*Kc*	Frequency	o - c
4	0	4	5	1	5	3333.1820	0.0000	2	2	0	2	1	1	3334.4716	0.0000
3	0	3	4	1	4	3333.2774	-0.0005	2	2	1	2	1	2	3334.5208	0.0002
2	1	1	2	2	0	3333.3583	-0.0002	3	2	2	3	1	3	3334.5461	0.0001
2	0	2	3	1	3	3333.3782	0.0001	4	1	4	3	0	3	3334.5540	0.0003
3	1	2	3	2	1	3333.3782	0.0002	6	0	6	5	1	5	3334.5717	-0.0003
4	1	4	5	0	5	3333.4031	0.0005	4	2	3	4	1	4	3334.5805	0.0002
1	0	1	2	1	2	3333.4849	0.0000	5	2	4	5	1	5	3334.6233	-0.0004
3	1	3	4	0	4	3333.5493	0.0001	5	1	5	4	0	4	3334.6489	-0.0004
0	0	0	1	1	1	3333.6000	0.0004	7	0	7	6	1	6	3334.7108	0.0001
4	0	4	4	1	3	3333.6260	0.0000	6	1	6	5	0	5	3334.7430	0.0001
3	0	3	3	1	2	3333.6676	0.0000	2	2	1	1	1	0	3334.7494	-0.0004
2	0	2	2	1	1	3333.6962	-0.0002	2	2	0	1	1	1	3334.7672	-0.0004
2	1	2	3	0	3	3333.6962	0.0004	7	1	7	6	0	6	3334.8372	0.0000
1	0	1	1	1	0	3333.7144	0.0002	3	2	2	2	1	1	3334.8642	-0.0001
1	1	1	2	0	2	3333.8391	-0.0005	3	2	1	2	1	2	3334.9196	-0.0001
2	0	2	1	1	1	3333.9921	-0.0004	4	2	3	3	1	2	3334.9698	-0.0004
1	1	0	1	0	1	3334.1183	0.0004	5	2	4	4	1	3	3335.0680	0.0003
2	1	1	2	0	2	3334.1356	0.0001	4	2	2	3	1	3	3335.0862	0.0002
3	0	3	2	1	2	3334.1356	-0.0005	6	2	5	5	1	4	3335.1576	0.0002
3	1	2	3	0	3	3334.1645	0.0005	7	2	6	6	1	5	3335.2400	0.0000
4	1	3	4	0	4	3334.2058	0.0004	5	2	3	4	1	4	3335.2705	0.0002
1	1	1	0	0	0	3334.2326	0.0000	3	3	1	2	2	0	3335.2743	0.0002
5	1	4	5	0	5	3334.2619	-0.0002	3	3	0	2	2	1	3335.2748	-0.0004
4	0	4	3	1	3	3334.2825	0.0001	8	2	7	7	1	6	3335.3166	0.0000
6	1	5	6	0	6	3334.3358	0.0000	4	3	2	3	2	1	3335.4032	0.0004
2	1	2	1	0	1	3334.3471	-0.0001	4	3	1	3	2	2	3335.4086	0.0002
6	2	4	6	1	5	3334.3990	-0.0001	6	2	4	5	1	5	3335.4761	0.0002
5	2	3	5	1	4	3334.4108	0.0001	5	3	3	4	2	2	3335.5272	-0.0001
5	0	5	4	1	4	3334.4287	0.0001	6	3	4	5	2	3	3335.6448	-0.0002
4	2	2	4	1	3	3334.4293	-0.0003	6	3	3	5	2	4	3335.6845	-0.0001
3	2	1	3	1	2	3334.4514	0.0001	7	2	5	6	1	6	3335.7059	0.0001
3	1	3	2	0	2	3334.4537	0.0000	6	4	3	5	3	2	3336.0508	-0.0001

The (1σ) RMS deviation for the fit of the *A*-state is 0.00026 cm^{-1}.

TABLE 2
***A*-State Ground State Combination Differences of $^{14}N_2$–CH_3CCH (cm^{-1})**

Upper			Lower			Observed	
J	*Ka*	*Kc*	*J*	*Ka*	*Kc*	Frequency	o - c
2	1	2	1	1	0	0.2286	-0.0007
2	1	2	1	1	0	0.2295	0.0002
2	1	1	1	1	1	0.2956	-0.0005
2	1	1	1	1	1	0.2959	-0.0002
3	1	3	2	1	1	0.3180	-0.0002
3	1	3	2	1	1	0.3181	-0.0001
4	1	4	3	1	2	0.3893	-0.0005
4	1	4	3	1	2	0.3902	0.0004
2	0	2	0	0	0	0.3935	0.0005
5	1	5	4	1	3	0.4440	0.0000
5	1	5	4	1	3	0.4447	0.0007
3	1	2	2	1	2	0.4680	-0.0004
3	1	2	2	1	2	0.4682	-0.0002
3	1	3	1	1	1	0.6139	-0.0004
3	0	3	1	0	1	0.6509	-0.0005
4	1	3	3	1	3	0.6565	0.0001
4	1	3	3	1	3	0.6569	0.0005
2	2	0	2	0	2	0.7773	0.0003
3	2	1	3	0	3	0.7863	0.0008
4	1	4	2	1	2	0.8582	0.0000
5	1	4	4	1	4	0.8597	0.0001
4	0	4	2	0	2	0.9044	-0.0001
6	1	5	5	1	5	1.0771	0.0003
5	1	5	3	1	3	1.1005	0.0001
5	0	5	3	0	3	1.1509	-0.0002

The (1σ) RMS deviation for the fit of the *A*-state ground state combination differences is 0.00039 cm^{-1}.

However, the final values of the molecular constants, whether from fitting with *B* and *C* varied, or with $(B + C)/2$ and $(B - C)/2$ varied, turn out to be indistinguishable.

To fit the infrared spectra we use the Hamiltonian shown in Eq. [2]. It is based on the work of Kilb *et al.* (*13*) with modifications to the centrifugal distortion terms suggested by Fraser *et al.* (*3*) and Rohart (*14*). This Hamiltonian was also used in the argon–propyne work (*2*).

$$\begin{aligned} H = {} & \nu_0 + [A - \tfrac{1}{2}(B + C)]\mathbf{J}_a^2 + \tfrac{1}{2}(B + C)\mathbf{J}^2 \\ & + \tfrac{1}{2}(B - C)(\mathbf{J}_b^2 - \mathbf{J}_c^2) - \Delta_J\mathbf{J}^4 - \Delta_{JK}\mathbf{J}^2\mathbf{J}_a^2 - \Delta_K\mathbf{J}_a^4 \\ & - 2\delta_J\mathbf{J}^2(\mathbf{J}_b^2 - \mathbf{J}_c^2) - \delta_K[\mathbf{J}_a^2(\mathbf{J}_b^2 - \mathbf{J}_c^2) \\ & + (\mathbf{J}_b^2 - \mathbf{J}_c^2)\mathbf{J}_a^2] + G(\mathbf{J}_a\mathbf{J}_b + \mathbf{J}_b\mathbf{J}_a) \\ & - 2(Q\mathbf{J}_a\mathbf{j} + N\mathbf{J}_b\mathbf{j}) + F_{\mathrm{Me}}\mathbf{j}^2 - \Delta_{Jm}\mathbf{J}^2\mathbf{j}^2 \\ & - \Delta_{Km}\mathbf{J}_a^2\mathbf{j}^2 - \Delta_{JKm}\mathbf{J}^2\mathbf{J}_a\mathbf{j} - \delta_m\mathbf{j}^2(\mathbf{J}_b^2 - \mathbf{J}_c^2) \\ & - \Delta_{K3m}\mathbf{J}_a^3\mathbf{j} - \delta_{Km}[\mathbf{J}_a(\mathbf{J}_b^2 - \mathbf{J}_c^2) + (\mathbf{J}_b^2 - \mathbf{J}_c^2)\mathbf{J}_a]\mathbf{j}, \end{aligned} \quad [2]$$

where

$$A = \left(1 + \frac{\lambda_a^2 I_\alpha}{r I_a}\right)\frac{\hbar}{4\pi I_a} \quad [3]$$

$$B = \left(1 + \frac{\lambda_b^2 I_\alpha}{r I_b}\right)\frac{\hbar}{4\pi I_b} \quad [4]$$

$$C = \frac{\hbar}{4\pi I_c} \quad [5]$$

$$Q = \frac{\lambda_a \hbar}{4\pi I_a} \quad [6]$$

$$N = \frac{\lambda_b \hbar}{4\pi I_b} \quad [7]$$

$$G = \frac{I_\alpha \lambda_a \lambda_b \hbar}{4\pi r I_a I_b} \quad [8]$$

$$r = 1 - \frac{\lambda_a^2 I_\alpha}{I_a} - \frac{\lambda_b^2 I_\alpha}{I_b} \quad [9]$$

$$F_{\mathrm{Me}} = \frac{\hbar}{4\pi r I_\alpha}. \quad [10]$$

The λ_i are the direction cosines between the symmetry axis of CH_3CCH and the *i* principal axis of the cluster, I_α is the moment of inertia of the CH_3 group about the monomer symmetry axis, $\mathbf{j}$ is the angular momentum operator for the internal rotation of CH_3CCH about its symmetry axis, and F_{Me} is the corresponding rotational constant. The terms $Q\mathbf{J}_a\mathbf{j}$ and $N\mathbf{J}_b\mathbf{j}$ are Coriolis interactions between the total angular momentum of the cluster and that of the internal methyl rotor, and *G* mixes cluster and methyl internal rotor angular momenta about the *a* and *b* principal axes of the cluster. The F_{Me} value used in the analysis of the spectra is derived by dividing the A_0 value of CH_3CCH by the *r* value shown in Eq. [2]. The value used in the analysis, F_{Me} = 157 740.0 MHz, is fixed in both the upper and the lower state. *G* is also fixed at a value determined from a calculation using the structural data and Eq. [9]. The product basis set $|J,$

TABLE 3
Observed *E*-State Infrared Transitions of $^{14}N_2$–CH_3CCH (cm^{-1})

Upper			Lower			Observed		Upper			Lower			Observed	
J	*Ka*	*Kc*	*J*	*Ka*	*Kc*	Frequency	o - c	*J*	*Ka*	*Kc*	*J*	*Ka*	*Kc*	Frequency	o - c
3	1	3	4	1	3	3333.1096	0.0004	2	2	1	2	1	2	3334.5030	-0.0003
3	0	3	4	1	4	3333.1574	0.0001	3	1	3	2	0	2	3334.5317	0.0003
2	0	2	3	1	3	3333.2975	-0.0002	4	1	3	4	0	4	3334.5778	0.0000
2	1	2	3	1	2	3333.2975	0.0007	3	2	2	3	1	3	3334.5836	0.0001
3	0	3	3	1	2	3333.3285	0.0002	2	2	1	1	1	0	3334.6233	-0.0001
1	0	1	2	1	2	3333.4505	-0.0007	4	1	4	3	0	3	3334.6732	0.0008
1	0	1	1	1	0	3333.5711	-0.0004	4	2	3	4	1	4	3334.6758	0.0003
0	0	0	1	1	1	3333.6107	-0.0002	4	1	3	3	1	3	3334.7196	-0.0005
2	1	1	3	1	3	3333.7698	-0.0004	3	2	2	2	1	1	3334.7266	0.0001
2	1	2	3	0	3	3333.8824	0.0000	2	2	1	1	1	1	3334.7295	-0.0004
3	0	3	2	1	2	3333.9464	0.0002	2	2	0	1	1	0	3334.7805	-0.0004
1	1	1	2	0	2	3333.9684	0.0006	5	1	5	4	0	4	3334.7993	-0.0007
3	1	3	2	1	1	3334.0583	0.0000	4	2	3	3	1	2	3334.8846	-0.0001
1	1	1	0	0	0	3334.2175	0.0004	3	2	1	2	1	1	3334.8832	-0.0004
1	1	0	1	0	1	3334.2574	0.0014	2	2	0	1	1	1	3334.8874	0.0000
3	2	2	3	1	2	3334.3019	0.0004	5	1	4	4	1	4	3334.8946	-0.0001
2	2	1	2	1	1	3334.3101	-0.0004	3	2	2	2	1	2	3334.9196	0.0002
2	1	1	1	1	1	3334.3330	0.0002	5	2	4	4	1	3	3334.9812	-0.0003
2	1	2	1	0	1	3334.3776	0.0004	4	2	2	3	1	2	3335.0243	0.0001
2	2	0	2	1	1	3334.4678	-0.0002	4	2	2	3	1	3	3335.3065	0.0005
4	2	2	4	1	3	3334.5000	-0.0002	3	3	0	2	2	0	3335.3110	0.0002

The (1σ) RMS deviation for the fit of the *E*-state is 0.00045 cm^{-1}.

$K_a, K_c\rangle \exp(im\alpha)/\sqrt{2\pi}$ is used to calculate the eigenvalues and eigenvectors of Eq. [2], where $|J, K_a, K_c\rangle$ are the prolate symmetric top wavefunctions and $\exp(im\alpha)/\sqrt{2\pi}$ are the internal rotor wavefunctions in the zero barrier limit. Further details of how the Hamiltonian matrix is set up are given in Ref. (*2*).

As stated above, the microwave spectra clearly show a splitting due to tunneling of the N_2 molecule, but the infrared spectrum shows no such splitting. Therefore, in fitting the $^{14}N_2$–CH_3CCH *A*-state infrared lines (Table 1) we used weighted averages of the *A*- and *B*-state microwave ground state constants given in Table 11, and allowed only the upper vibrational state parameters to vary. The Coriolis interaction constants *Q* and *N* and those centrifugal distortion constants that depend on *m* were fit in the following manner. Since no *E*-state microwave data were collected, we obtained ground state combination differences (see Table 4) from the *E*-state infrared transitions that were observed, and fit *Q*, *N*, and the $m \neq 0$ distortion constants with the remaining constants fixed at their *A*-state values. These values were then fixed and the *E*-state transitions were used to fit the upper state *Q*, *N*, and $m \neq 0$ distortion constants, with the excited state *A*-state constants fixed at the values from the fit to the infrared *A*-state transitions. The results of this fitting procedure are shown in Table 14. Note that the barrier to methyl internal rotation is assumed to be zero in these fits.

In both Ar–propyne (*2*) and N_2–propyne the ν_1 band origin is red shifted from that of the propyne monomer. However, the shift in N_2–propyne is 1.1431 cm^{-1} in the

TABLE 4
***E*-State Ground State Combination Differences of $^{14}N_2$–CH_3CCH (cm^{-1})**

Upper			Lower			Observed	
J	*Ka*	*Kc*	*J*	*Ka*	*Kc*	Frequency	o - c
1	1	0	1	1	1	0.10616	-0.0003
1	1	0	1	1	1	0.10691	0.0004
2	1	2	1	1	0	0.12029	0.0002
2	1	2	1	1	0	0.12053	0.0004
4	0	4	3	1	3	0.14187	-0.0005
3	1	3	2	1	1	0.14305	-0.0001
4	1	4	3	1	2	0.17055	-0.0004
4	1	4	3	1	2	0.17113	0.0001
2	1	1	2	1	2	0.19296	0.0001
2	1	2	1	1	1	0.22645	-0.0002
2	0	2	0	0	0	0.24908	-0.0002
3	1	2	3	1	3	0.28168	-0.0002
3	1	2	3	1	3	0.28229	0.0004
1	1	1	0	0	0	0.30312	0.0002
2	1	1	1	1	0	0.31325	0.0003
3	1	3	2	1	2	0.33601	0.0000
2	1	1	1	1	1	0.41941	0.0000
2	1	1	1	1	1	0.41961	0.0002
3	1	2	2	1	1	0.42473	-0.0003
3	1	2	2	1	1	0.42483	-0.0002
2	1	1	2	0	2	0.47340	0.0003
3	0	3	1	0	1	0.49520	0.0004
4	1	3	3	1	2	0.52428	0.0003
3	1	3	1	1	1	0.56317	0.0006
3	1	2	3	0	3	0.58492	-0.0007
3	1	2	2	1	2	0.61769	-0.0002
3	1	2	2	1	2	0.61785	0.0000
4	1	4	2	1	2	0.78898	0.0001
4	1	3	3	1	3	0.80657	0.0007
4	1	3	2	1	1	0.94865	-0.0004
3	1	2	1	0	1	1.08012	-0.0003
4	1	3	2	0	2	1.42205	0.0000

The (1σ) RMS deviation for the fit of the *E*-state ground state combination differences is 0.00028 cm^{-1}.

A-state and is 1.1456 cm^{-1} in the *E*-state. In Ar–propyne this shift is only 0.5351 cm^{-1} in the *A*-state and 0.5196 cm^{-1} in the *E*-state. Thus, the shift is more than twice as much for N_2–propyne as for Ar–propyne, and this probably reflects a stronger binding in the N_2 cluster. The changes in rotational constants upon excitation of the ν_1 band are not large. The *A* constants decrease by about 15 MHz in N_2–propyne, and by 20 MHz in Ar–propyne. The $(B + C)/2$ constant decreases by some 0.8 MHz in N_2–propyne, but only 0.03 MHz in Ar–propyne. The $(B - C)/2$ constant decreases by 0.3 MHz in N_2–propyne, but actually increases by 0.5 MHz in Ar–propyne. These changes are so small that they imply insignificant structural changes upon vibrational excitation of the acetylenic proton.

We are also interested in determining the barriers to internal rotation for the individual molecules within the cluster. We add a potential term to the Hamiltonian given in Eq. [2] of the form

$$V_{Me} = V_3(1 - \cos 3\alpha)/2 \qquad [11]$$

to determine the barrier for the internal rotation of the methyl top in the cluster. Introducing a nonzero barrier height produces a Hamiltonian matrix with a series of nonzero terms that couple all blocks where *m* differs by 3 (see Ref. *2*). We found that attempting to adjust V_3 in the fit did not lead to a convergent value. This may be due to the fact that we lack precise *E*-state microwave data. However, it was possible to place an upper limit of about 10 cm^{-1} on this barrier in the following way. In fitting the infrared, *E*-state GSCDs there is a rather strong correlation between the barrier to methyl rotation, and the *Q* and *N* constants. Thus, we chose to fix the barrier at some arbitrary value, and then do the fitting allowing the other *E*-state constants to vary. This was done at a series of fixed values for the barrier, and the results were compared. In general, a larger value for the barrier requires larger values for *Q* and *N*. Approaching a value of 10 cm^{-1} for the V_3 barrier turns out to require an *N* value that is quite close to the *B* rotational constant. Since *B* is an upper limit for *N*, we conclude that 10 cm^{-1} is an approximate upper limit for the threefold barrier in N_2–propyne. We feel that the actual methyl barrier is probably substantially less than 10 cm^{-1}. Note also that the Hamiltonian used in this fitting process assumes that the rest of the cluster is rigid; however, we know that the N_2 can also undergo internal rotation within the cluster, though with substantially higher barrier than for the methyl group.

Our experimental value for the barrier to methyl rotation is substantially lower than either of the two values

TABLE 5
Observed *A*-State (I = 0, 2) Microwave Transitions of $^{14}N_2$–CH_3CCH (MHz)

Upper					Lower					Observed		Center
J	*Ka*	*Kc*	*F*	*I*	*J*	*Ka*	*Kc*	*F*	*I*	Frequency	o - c	Frequency
1	1	1	2	2	0	0	0	2	2	9496.583	-0.001	9497.732
1	1	1	1	0	0	0	0	2	2	9496.729	-0.002	9497.732
1	1	1	1	0	0	0	0	0	0	9496.729	-0.002	9497.732
1	1	1	3	2	0	0	0	2	2	9498.063	0.003	9497.732
1	1	1	1	2	0	0	0	2	2	9499.883	0.001	9497.732
2	1	2	2	0	1	0	1	2	2	12933.188	0.003	12934.518
2	1	2	2	0	1	0	1	1	0	12933.229	-0.006	12934.518
2	1	2	3	2	1	0	1	2	2	12933.498	-0.010	12934.518
2	1	2	3	2	1	0	1	3	2	12934.017	0.006	12934.518
2	1	2	4	2	1	0	1	3	2	12934.931	-0.007	12934.518
2	1	2	1	2	1	0	1	1	2	12935.798	0.007	12934.518
2	1	2	2	2	1	0	1	1	2	12935.967	0.007	12934.518
3	1	3	3	0	2	0	2	2	0	16131.735	0.003	15133.030
3	1	3	4	2	2	0	2	3	2	16132.290	0.000	16133.030
3	1	3	5	2	2	0	2	4	2	16133.481	-0.001	16133.030
3	1	3	3	2	2	0	2	2	2	16133.874	-0.002	16133.030
2	2	0	3	2	2	1	1	3	2	16709.313	0.007	16710.495
2	2	0	4	2	2	1	1	4	2	16711.121	0.032	16710.495
2	2	0	2	2	2	1	1	2	2	16711.822	-0.038	16710.495
3	2	1	4	2	3	1	2	4	2	16106.220	-0.012	16106.956
3	2	1	5	2	3	1	2	5	2	16107.450	0.012	16106.956
4	0	4	2	2	3	1	3	1	2	10984.293	0.000	10985.104
4	0	4	4	2	3	1	3	3	2	10984.525	0.000	10985.104
4	0	4	6	2	3	1	3	5	2	10984.765	0.001	10985.104
4	0	4	5	2	3	1	3	4	2	10985.611	-0.002	10985.104

The (1σ) RMS deviation of the fit is 0.011 MHz.

derived from the distributed multipole analysis (DMA) given in Ref. (*1*). The electrostatic DMA alone predicts a value of 60 cm^{-1} and if the full DMA with dispersion effects is used, the barrier is predicted to be 40 cm^{-1}. The difference between the value estimated from the experimental data and that calculated from DMA may be associated with the rather large difference in the center-of-mass separations determined from experiment (3.708 Å) and calculation (3.38 Å). It was speculated that the larger experimental distance is due to the large-amplitude motions of the N_2 moiety.

The N_2 rotation barrier was estimated using a program that fit both *A*- and *B*-state microwave transitions of the $m = 0$ internal rotor state simultaneously. The Hamiltonian used was similar to that for internal methyl rotation, but with the $m \neq 0$ centrifugal distortion terms dropped. This Hamiltonian assumes that the axis of N_2 rotation lies in the plane of the heavy atoms:

TABLE 6
Observed *B*-State ($I = 1$) Microwave Transitions of $^{14}N_2$–CH_3CCH (MHz)

Upper					Lower					Observed		Center
J	*Ka*	*Kc*	*F*	*I*	*J*	*Ka*	*Kc*	*F*	*I*	Frequency	o - c	Frequency
1	1	1	0	1	0	0	0	1	1	9490.044	-0.004	9491.686
1	1	1	2	1	0	0	0	1	1	9491.523	0.002	9491.686
1	1	1	1	1	0	0	0	1	1	9492.504	0.002	9491.686
2	1	2	1	1	1	0	1	0	1	12927.323	-0.012	12928.430
2	1	2	3	1	1	0	1	2	1	12928.223	0.009	12928.430
2	1	2	2	1	1	0	1	2	1	12928.909	-0.008	12928.430
2	1	2	2	1	1	0	1	1	1	12929.254	0.011	12928.430
3	1	3	2	1	2	0	2	1	1	16126.387	-0.002	16126.998
3	1	3	4	1	2	0	2	3	1	16126.773	0.001	16126.998
3	1	3	3	1	2	0	2	2	1	16127.707	0.001	16126.998
4	0	4	4	1	3	1	3	3	1	10989.205	0.001	10989.714
4	0	4	5	1	3	1	3	4	1	10989.888	0.004	10989.714
4	0	4	3	1	3	1	3	2	1	10990.116	-0.005	10989.714
2	2	0	3	1	2	1	1	3	1	16693.310	0.017	16693.587
2	2	0	2	1	2	1	1	2	1	16694.600	-0.017	16693.587

The (1σ) RMS deviation of the fit is 0.008 MHz.

TABLE 7
Observed Microwave Transitions of $^{14}N_2$–CH_3CCH (MHz)

						A-State ($I = 0, 2$)			*B*-State ($I = 1$)		
Upper			Lower			Observed	o - c		Observed	o - c	
J	*Ka*	*Kc*	*J*	*Ka*	*Kc*	Frequency	a	b	Frequency	a	b
1	1	1	0	0	0	9497.732	-0.0064	-0.0383	9491.686	-0.0026	0.0151
4	0	4	3	1	3	10985.104	-0.0003	-0.0049	10989.714	-0.0002	0.0067
2	1	2	3	1	3	12934.518	0.0103	0.0085	12928.430	0.0044	0.0151
3	1	3	2	0	2	16133.030	-0.0043	0.0137	16126.998	-0.0018	-0.0240
3	2	1	3	1	2	16106.956	-0.0001				
2	0	2	2	1	1	16710.495	0.0001		16693.597	-0.0003	

a. Fit of *A* and *B*-states done separately. The *A*-state (1σ) RMS deviation is 0.0129 MHz; the *B*-state (1σ) RMS deviation is 0.0053 MHz.

b. Simultaneous fit of both *A* and *B*-states. The (1σ) RMS deviation is 0.0308 MHz.

TABLE 8
Observed Microwave Transitions of $^{15}N_2$–CH_3CCH (MHz)

						A-State ($I = 0$)			*B*-State ($I = 1$)		
Upper			Lower			Observed	o - c		Observed	o - c	
J	*Ka*	*Kc*	*J*	*Ka*	*Kc*	Frequency	a	b	Frequency	a	b
1	1	1	0	0	0	9383.644	0.0062	-0.0096	9378.961	-0.0002	0.0095
4	0	4	3	1	3	10375.573	0.0003	-0.0106	10379.207	-0.0001	0.0019
2	1	2	1	0	1	12711.457	-0.0100	-0.0041	12706.771	0.0003	0.0049
5	0	5	4	1	4				14627.859	0.0000	0.0086
5	2	3	5	1	4				15006.966	0.0011	-0.0197
4	2	2	4	1	3				15572.034	0.0011	0.0074
3	1	3	2	0	2	15815.046	0.0042	0.0210	15810.385	-0.0001	-0.0220
3	2	1	3	1	2	16209.919	0.0012	0.0083	16197.157	-0.0014	0.0147
2	2	0	2	1	1	16784.726	-0.0001	-0.0140	16771.693	0.0006	0.0017

a. Fit of *A* and *B*-states done separately. The *A*-state (1σ) RMS deviation is 0.0125 MHz; the *B*-state (1σ) RMS deviation is 0.0017 MHz.

b. Simultaneous fit of both *A* and *B*-states. The (1σ) RMS deviation is 0.015 MHz.

$$H_{\text{rot}} = \left(A_N - \left(\frac{B_N + C_N}{2}\right)\right)\mathbf{J}_a^2 + \left(\frac{B_N + C_N}{2}\right)\mathbf{J}^2 + \left(\frac{B_N - C_N}{2}\right)(\mathbf{J}_b^2 - \mathbf{J}_c^2) - \Delta_J\mathbf{J}^4 - \Delta_{JK}\mathbf{J}^2\mathbf{J}_a^2 - \Delta_K\mathbf{J}_a^4 - 2\delta_J\mathbf{J}^2(\mathbf{J}_b^2 - \mathbf{J}_c^2) - \delta_K[\mathbf{J}_a^2(\mathbf{J}_b^2 - \mathbf{J}_c^2) + (\mathbf{J}_b^2 - \mathbf{J}_c^2)\mathbf{J}_a^2] + G_N(\mathbf{J}_a\mathbf{J}_b + \mathbf{J}_b\mathbf{J}_a) - 2(Q_N\mathbf{J}_a\mathbf{j}_N + N_N\mathbf{J}_b\mathbf{j}_N) + F_N\mathbf{j}_N^2 + V_2(1 - \cos 2\alpha)/2. \quad [12]$$

The subscript *N* denotes spectroscopic constants that are obtained from a simultaneous fit of the *A*- and *B*-state microwave data. In general, the meanings are similar to those for methyl internal rotation. Starting values for these quantities are determined from the structural parameters and Eqs. [3] to [10]. It is assumed at this level of approximation that there is no methyl top internal rotation and changes in the principal moments of the cluster as the N_2 undergoes internal rotation are ignored. We have computed the Hamiltonian when both methyl and N_2 rotation are included, and it does not have large kinetic energy elements connecting these two types of internal rotation. An important caveat to this simplified approach is that, even though there seems to be little kinetic coupling of the CH_3 and N_2 rotations, there could still be a significant potential energy term connecting the two displacements.

It is fortuitous that the splitting between the *A*- and *B*-state energy levels is strongly dependent on the value of the K_a index. Since the data set consists of transitions with *b*-type selection rules, considerable splitting of the transitions is observed. Table 7 shows that this splitting ranges between about 5 and 20 MHz for N_2–CH_3CCH and is measurable with precision to better than 10 kHz. If the data set had consisted of only *a*-type transitions, determination of the N_2 barrier would have been much less precise. Up to $J = 4$, the largest *a*-type transition splitting is predicted to be about 0.7 MHz, with most around 0.2 or 0.3 MHz. Such small values would yield a barrier to internal rotation with substantially greater uncertainty than that obtained from the *b*-type transitions.

We consider two possible modes of N_2 rotation. In one, the axis of N_2 rotation is parallel to the *c* axis of the cluster; that is, the rotation is in the heavy atom plane. In the other, the rotation is about an axis that is nearly colinear with the *a* axis of the cluster; that is, the nitrogen rotates out of the heavy atom plane. Assuming in-plane rotation, it is not possible to get the standard deviation of the fit down below 1.0 MHz. For out-of-plane rotation the fit is considerably better with (1σ) RMS deviations of 0.067 MHz for $^{14}N_2$–

TABLE 9
Observed *A*-State ($I = 0$) Microwave Transitions of $^{15}N_2$–CH_3CCD (MHz)

Upper				Lower				Observed		Splitting	Center
J	*Ka*	*Kc*	*F*	*J*	*Ka*	*Kc*	*F*	Frequency	o - c	Frequency	Frequency
1	1	1	0	0	0	0	1	8698.713	-0.0034	-0.103	8698.816
1	1	1	2	0	0	0	1	8698.806	0.0000	-0.010	8698.816
1	1	1	1	0	0	0	1	8698.869	0.0032	0.053	8698.816
2	1	2	1	1	0	1	0	11943.923	0.0021	-0.079	11944.002
2	1	2	3	1	0	1	2	11943.990	-0.0004	-0.012	11944.002
2	1	2	2	1	0	1	1	11944.052	0.0002	0.050	11944.002
3	1	3	4	2	0	2	3	14954.809	0.0059	-0.006	14954.815
3	1	3	3	2	0	2	2	14954.848	-0.0066	0.033	14954.815

The *A*-state (1σ) RMS deviation is 0.0036 MHz.

CH_3CCH and 0.086 MHz for $^{15}N_2$–CH_3CCH. This fact suggests that the out-of-plane mode is responsible for the exchange of the nitrogen nuclei. This out-of-plane motion would have a substantially lower repulsion interaction with the carbons than the in-plane motion, for which the van der Waals spheres would overlap considerably (*1*).

In the fitting process, we began with the principal rotational constants that come from the molecular structure. Some changes of these are necessary in fitting the spectrum, as shown in Tables 15 and 16. We allowed the N_2 internal rotation centrifugal distortion constants to vary, but the changes found were all small: much smaller than the estimated standard deviations of the constants. Therefore all these terms were set to zero and not adjusted. The spectroscopic constant G_N, the coefficient of $(\mathbf{J}_a\mathbf{J}_b + \mathbf{J}_b\mathbf{J}_a)$, was also included. The three parameters A_N, B_N, and G_N are known to be linearly correlated; only two are independent. Conventionally, this interdependence is removed by a rotation of axes to give G_N a value of zero. We have not done this rotation of axes; rather, we fixed G_N at the value computed from the structure. The quantities A_N, Q_N, and V_2 are also interrelated and cause prob-

TABLE 10
Observed *B*-State ($I = 0$) Microwave Transitions of $^{15}N_2$–CH_3CCD (MHz)

Upper				Lower				Observed		Splitting	Center
J	*Ka*	*Kc*	*F*	*J*	*Ka*	*Kc*	*F*	Frequency	o - c	Frequency	Frequency
1	1	1	0	0	0	0	1	8694.888	-0.0024	-0.105	8694.993
1	1	1	2	0	0	0	1	8694.984	0.0013	0.009	8694.993
1	1	1	1	0	0	0	1	8695.046	0.0017	0.053	8694.993
2	1	2	1	1	0	1	0	11940.072	0.0009	0.081	11940.153
2	1	2	3	1	0	1	2	11940.142	0.0010	0.011	11940.153
2	1	2	2	1	0	1	1	11940.202	-0.0023	0.049	11940.153
3	1	3	4	2	0	2	3	14950.985	0.0024	0.010	14950.995
3	1	3	3	2	0	2	2	14951.034	-0.0022	0.039	14950.995

The *B*-state (1σ) RMS deviation is 0.0019 MHz.

TABLE 11
Fit Parameters for $^{14}N_2$–CH_3CCH (MHz)

	A-State ($I = 0, 2$)	*B*-State ($I = 1$)
A	7779.201 (17)[a]	7773.110 (6)[a]
$(B+C)/2$	1969.0646 (16)	1968.9768 (8)
$(B-C)/2$	250.480 (6)	250.416 (3)
Δ_J	0.01719 (fix)	0.01719 (fix)
Δ_{JK}	0.1018 (15)	0.0978 (15)
Δ_K	-0.0258 (36)	-0.08310 (fix)
δ_J	0.00377 (fix)	0.00377 (fix)
δ_K	0.09220 (fix)	0.09220 (fix)
eQq_{aa}	1.118(52)	1.087(75)
eQq_{bb}	-3.281(20)	-3.273(28)
eQq_{cc}	2.163(48)	2.186(70)

a. Uncertainties shown in parentheses refer to the last digit(s) and are one standard deviation.

TABLE 13
Fit Parameters for $^{15}N_2$–CH_3CCD (MHz)

	A-State ($I = 0$)	*B*-State ($I = 1$)
A	7076.058[a]	7072.203[a]
$(B+C)/2$	1870.655	1870.5943
$(B-C)/2$	247.876	247.839
Δ_J	0.0172 (fix)	0.0172 (fix)
Δ_{JK}	0.0950 (fix)	0.0895 (fix)
Δ_K	-0.0380 (fix)	-0.0831 (fix)
δ_J	0.00377 (fix)	0.00377 (fix)
δ_K	0.0920 (fix)	0.0920 (fix)
eQq_{aa}	-0.1253(167)	-0.1253(167)
eQq_{bb}	0.1993(61)	0.1993(61)
eQq_{cc}	-0.0740(191)	-0.0740(191)

a. Only three rotational transitions were measured for this isotopic species, so this is an exact fit and the uncertainties cannot be determined.

lems when they are all allowed to vary independently. The quantities N_N and Q_N were fixed close to their values from the structure; V_2 was fixed at various values. Then A_N, $(B_N + C_N)/2$, $(B_N - C_N)/2$, and a few of the Watson centrifugal distortion constants were varied. The *A*- and *B*-state splittings were found to depend strongly on V_2, and weakly on other parameters. So we adjusted V_2 to obtain an optimal fit to the splittings. Finally, we allowed the A_N and $(B_N + C_N)/2$ constants to differ in the *A*- and *B*-states; this produced an important improvement in the fit, though the differences required are quite small. Final values of the adjusted parameters are shown in Table 15 for $^{14}N_2$–CH_3CCH and in Table 16 for $^{15}N_2$–CH_3CCH. Barriers for the $^{15}N_2$ and $^{14}N_2$ species are quite similar, with values of 70.8 and 71.0 cm^{-1}, respectively. Use of a Q constant some 10% smaller gave barriers lower by only 1.5 cm^{-1}. For $^{14}N_2$ a curious problem was encountered in the fitting. The two highest lines, near 16 700 MHz, had much higher deviations in the fit: over 1.0 MHz. So we removed them and obtained a better fit, though not as good as that for $^{15}N_2$. In the latter species the corresponding transitions, $2_{20} \leftarrow 2_{11}$, had deviations comparable to those of the other lines and were thus included in the fit. Since we have so few transitions for $^{15}N_2$–CH_3CCD, it was not possible to determine a barrier to N_2 rotation for this cluster.

TABLE 12
Fit Parameters for $^{15}N_2$–CH_3CCH (MHz)

	A-State ($I = 0$)	*B*-State ($I = 1$)
A	7719.559 (17)[a]	7714.847 (2)[a]
$(B+C)/2$	1899.0186 (15)	1898.9558 (7)
$(B-C)/2$	234.918 (6)	234.8782 (57)
Δ_J	0.01719 (fix)	0.017216 (60)
Δ_{JK}	0.0950 (14)	0.08954 (46)
Δ_K	-0.0379 (35)	-0.08302 (73)
δ_J	0.00377 (fix)	0.003821 (90)
δ_K	0.0920 (fix)	0.09284 (194)

a. Uncertainties shown in parentheses refer to the last digit(s) and are one standard deviation.

Calculations of the Hamiltonian coefficients from assumed structures showed significant changes as the N_2 molecule was set to various out-of-plane angles, with fixed center-of-mass separation of N_2 and propyne. In principle such changes would require additional terms in the molecular constants (see Eqs. [3]–[9]), giving a dependence of rotational parameters on the N_2 out-of-plane angle. A further problem would likely be a change in the minimum energy center-of-mass distance as N_2 rotates. However, the total

TABLE 14
Fit Parameters for $^{14}N_2$–CH_3CCH (MHz)

	v = 1[a]	v = 0
A	7762.35 (89)[b]	7777.169 (8)[b]
$(B+C)/2$	1968.225 (63)	1969.034 (4)
$(B-C)/2$	250.145 (48)	250.454 (3)
Δ_J	0.0099 (56)	0.01719 (fix)
Δ_{JK}	0.115 (35)	0.102 (1)
Δ_K	-0.117 (94)	-0.0482 (16)
δ_J	-0.0078 (48)	0.00377 (fix)
δ_K	0.25 (13)	0.09220 (fix)
F_{Me}	157740.0 (fix)	157740.0 (fix)
N	1926.0 (12)	1926.9 (32)
Q	603.8 (20)	601.2 (37)
Δ_{Jm}	7.84 (28)	8.59 (76)
Δ_{Km}	-8.2 (13)	10.1 (98)
Δ_{JKm}	1.44 (34)	8.9 (40)
δ_{Jm}	5.21 (36)	3.66 (64)

a. The fit band origins are 3333.9163(1) cm^{-1} for the *A*-state and 3333.9138 cm^{-1} for the *E*-state.

b. Uncertainties shown in parentheses refer to the last digit(s) and are one standard deviation.

number of experimental observations was far too small for inclusion of such additional terms. We conclude that most values obtained in the fitting process should be regarded as ''effective'' and representing some suitable average over the course of the N_2 rotation (or out-of-plane vibration). The barrier that we obtained is consistent with an out-of-plane vibration of about 22 cm^{-1}. A simple calculation for harmonic angular vibration yields about 28° for the vibrational angle amplitude.

There are five van der Waals modes for N_2–CH_3CCH, namely, the center-of-mass stretching mode with force constant k_s; a bending mode where the center-of-mass of the N_2 molecule moves approximately parallel to the *b* axis of the cluster (k_b); the in-plane N_2 twisting motion, or *c*-twist, ($k_{c\text{-}tw}$); the out-of-plane twisting motion, or *a*-twist ($k_{a\text{-}tw}$); and the internal rotation of the methyl top (k_{Me}). The out-of-plane twist and the methyl top rotation have symmetries different from those of the other vibrations and no interactions are expected between the former vibrations and the latter. There are, therefore, three diagonal and three off-diagonal force constants, the latter coupling the stretching, the bending, and the in-plane twist motions. The program ASYM20 of Hedberg and Mills (*15*) was used to estimate the stretching and bending force constants, k_s and k_b. In general, these estimates were made by using the structural information about the cluster, force constants for the monomers, and trial guesses for the force constants as input to the program, and then using the program to calculate the quartic distortion constants. These calculated values were compared to the experimental values and the procedure was repeated until there was a reasonable convergence between the two sets of values. Further details are given below.

At first N_2 was regarded as a point mass with a value of 28 amu sitting at the center-of-mass of the $^{14}N_2$ subunit. The stretching force constant for each bond in the CH_3CCH unit was included to take into account the nonrigidity of the propyne. Only the stretching and bending force constants and the stretch–bend interaction force constant were used. With these input parameters and the structure of the cluster, the force constant values that gave the best estimates of the distortion constants were $k_s = 0.0195$ mdyn/Å and $k_b = 0.0271$ mdyn/Å with an interaction constant of -0.001 mdyn/Å. The calculated stretching frequency is 47.2 cm^{-1} and the bending frequency is 41.8 cm^{-1}. The resulting Watson quartic distortion constants are $\Delta_J = 17.1$ kHz, $\Delta_{JK} = 97.7$ kHz, $\Delta_K = -83.3$ kHz, $\delta_J = 3.5$ kHz, and $\delta_K = 87.1$ kHz, compared to the experimental values of $\Delta_J = 17.2$ kHz, $\Delta_{JK} = 102$ kHz, $\Delta_K = -48.2$ kHz, $\delta_J = 3.77$ kHz, and $\delta_K = 92.2$ kHz.

In order to improve these results, $^{14}N_2$ was treated as a diatomic in the cluster with a stretching force constant of 22.949 mdyn/Å. The stretching, bending, and interaction force constants and the in-plane twisting force constant were included in the calculation. For the van der Waals stretching mode, the stretching force constant for each N atom is assumed to be equal. The best values for the force constants were found to be $k_s = 0.00990$ mdyn/Å, $k_b = 0.01018$ mdyn/Å, $k_{c\text{-}tw} = 0.00306$ mdyn/Å, and $k_{s,b} = -0.0008$ mdyn/Å. The calculated stretching frequency is 46 cm^{-1}, the bending frequency is 37.2 cm^{-1}, and the twisting frequency is 35.2 cm^{-1}. The resulting quartic centrifugal distortion constants are $\Delta_J = 16.9$ kHz, $\Delta_{JK} = 101.4$ kHz, $\Delta_K = -46.9$ kHz, $\delta_J = 3.88$ kHz, and $\delta_K = 91.9$ kHz, which are in good agreement with the experimental values.

An approximation to the van der Waals stretching constant can also be made using the diatomic approximation

$$\nu_s = 2\sqrt{(B^3/D_0)}. \qquad [13]$$

Since N_2–CH_3CCH is an asymmetric top $(B + C)/2$ is used instead of B and Δ_J is used instead of D_0. Inserting the values for $^{14}N_2$–CH_3CCH gives a stretching frequency of 42.3 cm^{-1} which is in good agreement with the calculated value.

TABLE 15
Fit Parameters for $^{14}N_2$–CH_3CCH (MHz): *A* and *B* States Fit Simultaneously

	Fit	Theoretical consts, from struct.
A_N	8637.076(18)[a]	8642.6
$(B_N+C_N)/2$	1979.501(10)	1958.1
$(B_N-C_N)/2$	261.389(6)	238.9
Δ_J	0.01778 (36)	
Δ_{JK}	0.27803 (fix)	
Δ_K	-0.39675 (fix)	
δ_J	0.0041 (fix)	
δ_K	0.092 (fix)	
F_N	67090.0(fix)	67090.0
G_N	135.0(fix)	135.0
N_N	1195.0(fix)	1191.0
Q_N	7600.0(fix)	7608.0
V_2	70.8 cm^{-1}	
ADF[b]	0.0541 (21)	
BPDF[b]	0.0156 (40)	

a. Uncertainties shown in parentheses refer to the last digit(s) and are one standard deviation.

b. ADF = *A*(*A*-state) - *A*(*B*-state) ; BPDF = (*B*+*C*)/2 (*A*-state) - (*B*+*C*)/2 (*B*-state)

Because more distortion constants were fit for $^{15}N_2$–CH_3CCH the force constants from its data set should be more accurate than that of $^{14}N_2$–CH_3CCH. Repeating the above analysis for the $^{15}N_2$ isotopic species gives k_s = 0.00886 mdyn/Å, k_b = 0.01018 mdyn/Å, $k_{c\text{-}tw}$ = 0.00262 mdyn/Å, and $k_{s,b}$ = −0.00012 mdyn/Å. The calculated stretching frequency is 41.9 cm^{-1}, the bending frequency is 37.8 cm^{-1}, and the twisting frequency is 31.6 cm^{-1}. The resulting quartic centrifugal distortion constants are Δ_J = 16.9 kHz, Δ_{JK} = 99.5 kHz, Δ_J = −33.4 kHz, δ_J = 3.74 kHz, and δ_K = 89.8 kHz. Compare these with the experimental values in Table 12.

CONCLUSION

The infrared spectrum of $^{14}N_2$–CH_3CCH in the 3.0-μm region has been observed and the rovibrational transitions have been assigned for the *A* (m = 0) and *E* (m = ±1) methyl top internal rotor states. The *E*-state transitions were used to estimate an upper limit to the barrier to internal rotation at 10 cm^{-1}. This estimate for the barrier height is reasonable when compared to the barrier heights of similar van der Waals clusters such as Ar–CH_3CCH, Ar–CH_3Cl, and Ar–CH_3CN.

The centers-of-gravity of the *A*-state microwave transitions of $^{14}N_2$–CH_3CCH, $^{15}N_2$–CH_3CCH, and $^{15}N_2$–CH_3CCD were observed to split into two groups of transitions due to the internal rotation of the N_2 molecule within the cluster. By comparing the quality of fits of this microwave splitting, assuming that the internal rotation is about an axis that is parallel to the *a* or *c* axis of the complex, it was determined that the internal motion of the N_2 moiety is about an axis connecting the centers-of-mass of the molecules in the cluster (roughly parallel with the *a* axis); i.e., the N_2 molecule rotates out of the heavy atom plane of the cluster. The splittings in the microwave spectra were fit to a barrier height of 71 cm^{-1} for the hindered N_2 motion.

TABLE 16
Fit Parameters for $^{15}N_2$–CH_3CCH (MHz): *A* and *B* States Fit Simultaneously

	Fit	Theoretical consts, from struct.
A_N	8632.919(4)[a]	8641.4
$(B_N+C_N)/2$	1909.4692(9)	1888.2
$(B_N-C_N)/2$	246.224(2)	224.6
Δ_J	0.01716 (fix)	
Δ_{JK}	0.09293 (fix)	
Δ_K	-0.0607 (fix)	
δ_J	0.00428 (fix)	
δ_K	0.092 (fix)	
F_N	63090.0(fix)	63090.0
G_N	138.0(fix)	138.0
N_N	1155.0(fix)	1152.5
Q_N	7600.0(fix)	7612.4
V_2	71.0 cm^{-1}	
ADF[b]	0.0076 (43)	
BPDF[b]	0.0106 (17)	

a. Uncertainties shown in parentheses refer to the last digit(s) and are one standard deviation.

b. ADF = *A*(*A*-state) - *A*(*B*-state); BPDF = (*B*+*C*)/2 (*A*-state) - (*B*+*C*)/2 (*B*-state)

ACKNOWLEDGMENTS

We respectfully dedicate this work to the memory of our friend and colleague Professor David F. Eggers.

This work was supported by the National Science Foundation (Grant CHE-9015765) and a Pacific Northwest Laboratories Professorship (R.O.W.). R.D.B. thanks the Deutsche Forschungsgemeinschaft (Grant Be 1315/1-1) for the generous support he was given while working in Seattle.

REFERENCES

1. F. J. Lovas, P. W. Fowler, Z. Kisiel, S-H. Tseng, R. D. Beck, D. F. Eggers, T. A. Blake, and R. O. Watts, *J. Chem. Phys.* **100,** 3415–3421 (1994).
2. T. A. Blake, D. F. Eggers, S-H. Tseng, M. Lewerenz, R. P. Swift, R. D. Beck, and R. O. Watts, *J. Chem. Phys.* **98,** 6031–6043 (1993).
3. G. T. Fraser, R. D. Suenram, and F. J. Lovas, *J. Chem. Phys.* **86,** 3107–3114 (1987).
4. R. S. Ford, R. D. Suenram, G. T. Fraser, F. J. Lovas, and K. R. Leopold, *J. Chem. Phys.* **94,** 5306–5312 (1991).
5. C. V. Boughton, R. E. Miller, and R. O. Watts, *Aust. J. Phys.* **35,** 611–621 (1982); G. W. Bryant, D. F. Eggers, and R. O. Watts, *J. Chem. Soc. Faraday Trans. 2* **84,** 1443–1455 (1988).
6. B. H. Pate, K. K. Lehmann, and G. Scoles, *J. Chem. Phys.* **95,** 3891–3916 (1991).
7. A. McIllroy and D. J. Nesbitt, *J. Chem. Phys.* **91,** 104–113 (1989).
8. T. J. Balle and W. H. Flygare, *Rev. Sci. Instrum.* **52,** 33–45 (1981).
9. F. J. Lovas, R. D. Suenram, G. T. Fraser, C. W. Gillies, and J. Zozom, *J. Chem. Phys.* **88,** 722–729 (1988); R. D. Suenram, F. J. Lovas, G. T. Fraser, J. Z. Gillies, and M. Onda, *J. Mol. Spectrosc.* **137,** 127–137 (1989).
10. J. K. G. Watson, *in* ''Vibrational Spectra and Structure. A Series of Advances'' (J. R. Durig, Ed.), Vol. 6, pp. 1–88, Elsevier, New York, 1977.
11. H. O. Leung, M. D. Marshall, R. D. Suenram, and F. J. Lovas, *J. Chem. Phys.* **90,** 700–712 (1989).
12. W. H. Kirchhoff and D. R. Johnson, *J. Mol. Spectrosc.* **45,** 159–165 (1973).
13. R. W. Kilb, C. C. Lin, and E. B. Wilson, Jr., *J. Chem. Phys.* **26,** 1695–1703 (1957).
14. F. Rohart, *J. Mol. Spectrosc.* **57,** 301–311 (1975).
15. L. Hedberg and I. M. Mills, *J. Mol. Spectrosc.* **160,** 117–142 (1993).